Stem Cell Reports, Volume *7*

Supplemental Information

Glucose-Induced Oxidative Stress Reduces Proliferation in Embryonic Stem Cells via FOXO3A/β-Catenin-Dependent Transcription of *p21^{cip1}*

Darcie L. McClelland Descalzo, Tiffany S. Satoorian, Lauren M. Walker, Nicole R.L. Sparks, Polina Y. Pulyanina, and Nicole I. zur Nieden

Supplemental Information

Supplemental Experimental Procedures

Doubling Time

To determine the doubling time the natural logarithm of the cell number counted at time x was subtracted from the initial cell number and plotted against the hours after seeding. Doubling time was calculated from the slope of the straight line in the exponential growth stage.

AGE/RAGE

The percentage of cells positive for advanced glycation end products (AGE) and their receptors (RAGE), was determined from 4% formaldehyde fixed single cell suspensions (floating and attached population). Cells were stained with anti-AGE (Serotec) and anti-RAGE (Sigma Aldrich) antibodies diluted in PBS containing 10% FBS for 45 min at 4°C. Cells were then stained with secondary antibodies diluted in PBS containing 10% FBS for 45 min at 4°C. The percentage of positive cells was determined with a FC 500 flow cytometer (Beckman coulter) and 10,000 events were analyzed with appropriate scatter gates with the CXP software. The following secondary antibodies were used: anti-goat Alexa Flour 488 (Life Technologies, #A11078), anti-rabbit Alexa Fluor 546 (Life Technologies, #A11035).

Supplemental figure legends

Supplemental figure 1. (A) Doubling time of D3 cells were determined and confirmed that initial high Glc exposure led to a decrease in doubling time, with this being reversed following acute hyperglycemic exposure (5 days), n=3 independent replicates ± SD. **P*<0.05, Student's T-test compared to 5.5 mM Glc. (B) Reversal in cell numbers after initial (24h) and acute (5 days) Glc exposure confirmed in CCE murine ESCs; n=3 independent replicates ± SD. (C) Chronic hyperglycemic exposure *in vivo* results in modifications of proteins and lipids, forming advanced glycation end products (AGEs) that bind to receptors for these AGEs (RAGEs), resulting in an increase in oxidative damage to the cell. Exposure of ESCs to varying Glc conditions did not affect the generation of AGEs and RAGEs; n=3 independent replicates ± SD. (D) Changes in mRNA expression patterns of FOXO target genes *Sod2, Cat, p21^{cip1} and p27^{kip1}* were confirmed in CCE murine ESCs; quantitative PCR, n=3 independent replicates ± SD. **P*<0.05, One-Way ANOVA versus 5.5 mM Glc.

Supplemental figure 2. (A) Western blot analysis of cytoplasmic and nuclear cellular fractions show increased nuclear localization of FOXO1, FOXO3a and CTNNB1 upon Glc exposure. They also reveal that FOXO3a and CTNNB1 nuclear increases seem to be caused by altered shuttling of existing protein pools, while an increase in overall cellular FOXO1 protein may contribute to its higher nuclear levels. (B) Western blot analysis for FOXO1 and FOXO3a levels in whole cell lysates after transfection of ESCs with sh-*FoxO1/3* in comparison to wildtype cells (WT) confirm knockdown of both FOXOs in *sh-FoxO1/3* cells. TBP, TATA binding protein; WT, wildtype.

Supplemental figure 3. (A) Western blot showing the increased nuclear level of TCF7L1 in 25 mM Glc. (B) Changes in *Cat* mRNA expression patterns in murine ESCs with an overexpression of a dominant negative form of the CTNNB1 associated transcription factor TCF7L1 (Wu et al., 2012); suggest that TCF7L1 represses Cat expression. Quantitative PCR, n=3 independent replicates ± SD. **P*<0.05, One-Way ANOVA versus 5.5 mM Glc, $^{\Delta}P$<0.05, One-Way ANOVA compared to WT. DN, dominant-negative; TBP, TATA binding protein; WT, wildtype.

Supplemental figure 4. (A) RT-PCR analysis of *p53* expression in response to varying Glc conditions, pooled RNA from three independent experiments. (B) Western blot for the p53 protein on nuclear protein fractions and corresponding densitometry. The p53 antibody was from Abcam (#ab26). Regulation of proliferation via p21 is often associated with function of p53, a key transcriptional regulator of cell proliferation and death itself. In fact, $p21^{cip1}$ was identified as a classic p53 target when it was first described in 1993 (el-Deiry et al., 1993). In order to determine whether p53 contributed to the Glc-mediated effects on the cell cycle RT-PCR analysis was carried out for *p53*. The results demonstrated that while $p21^{cip1}$ expression was increased in a Glc-dependent manner (compare Figure 3B), *p53* expression was not. Although there was not an observable Glc-dependent effect on *p53* mRNA expression and no statistical difference observed between the levels of nuclear p53 protein between the 5.5 mM and 25 mM Glc, our study cannot conclusively answer whether the increase in $p21^{cip1}$ transcription was p53-independent. The p21-luc reporter used in Figure 3D lacked the p53 binding site and therefore reported on p53-independent activation of $p21^{cip1}$. However, p53 might still be contributing to overall $p21^{cip1}$ mRNA levels. (C) Hydrogen peroxide levels in ESCs treated with the PI3K inhibitor LY294002; n=3 independent replicates ± SD. **P*<0.05, One-Way ANOVA versus 5.5 mM Glc. To ensure that the observed results were due to altered AKT activity and not to upstream disruption of the insulin signaling pathway, cells were treated with the PI3K inhibitor LY294002. Although LY294002 treated cells displayed Glc dependent regulation of ROS, the observed pattern of regulation was the same as in LY294002 non-treated cells, indicating that the effects seen with AKT inhibition are in fact due to alteration of AKT activity and not to upstream PI3K activation. These results demonstrate that in the hyperglycemic environment, excess Glc inhibits activity of AKT leading to overexpression of FOXO3a, which increases expression and activity of downstream target genes protecting the cells from harmful ROS and decreasing cellular proliferation. DHR, dihydrorhodamine; Glc, glucose; TBP, TATA binding protein.

Supplemental tables

Table S1: Primers used for quantitative PCR, related to Figures 1-4

	Forward	Reverse	T_m°C
Cat	TGTTTATTCCTGTGCTGTGCGGTG	AAAGCAACCAAACACGGTCCTTCC	60
FoxO1	TATTGAGCGCTTGGACTGTG	CTGTGTGGGAAGCTTTGGTT	60
FoxO3a	GGGGAGTTTGGTCAATCAGA	GCCTGAGAGAGAGTCCGAGA	60
FoxO4	CAAGAAGAAGCCGTCTGTCC	CTGACGGTGCTAGCATTTGA	60
Sod2	TTACAACTCAGGTCGCTCTCA	GGCTGTCAGCTTCTCCCTTAAAC	60
$p21^{cip1}$	GAGTAGGACTTTGGGGTCTCCT	TGTCTTCACAGGTCTGAGCAAT	60

p27^{kip1}	GGATATGGAAGAAGCGAGTCAG	CCTGTAGTAGAACTCGGGCAAG	60
Tbp	CAGCCTTCCACCTTATGCTC	CCGTAAGGCATCATTGGACT	60

Table S2: ReChIP primer sets used in this study, related to Figure 5

	Forward	Reverse	T_m°C
p21^{cip1}	CTACCTGTCCACAAGTCATTTCC	GTCTTACTGCAGCGACAGAAAAGT	66
p27^{kip1}	TTTTTAAATAAAGGGGTCCCAGAC	TTAACATTTTCCCCAAGTGTTGTA	63
Sod2	ATGTAGTTAAGATGGCCTAAAAGC	GACAATTGTGTAACAAAAGGAACC	63

Supplemental Fig. 1

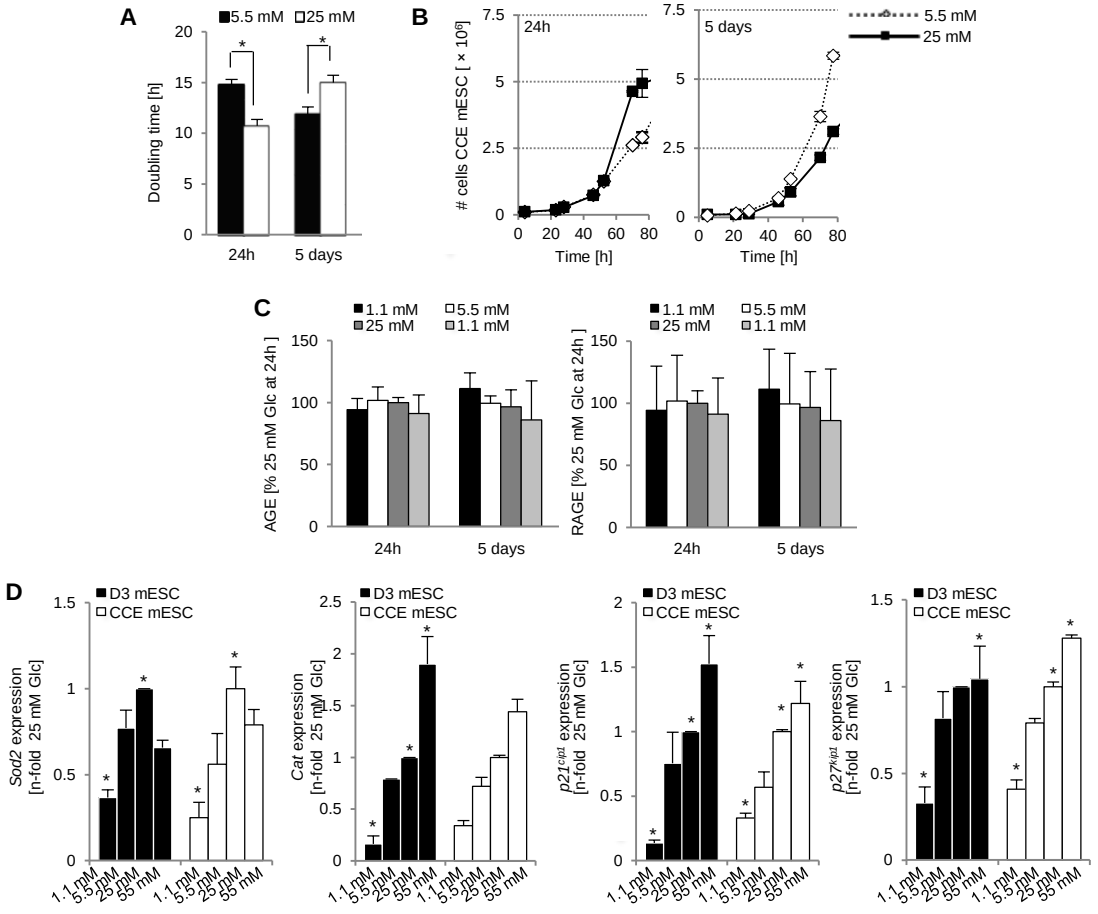

Supplemental Fig. 2

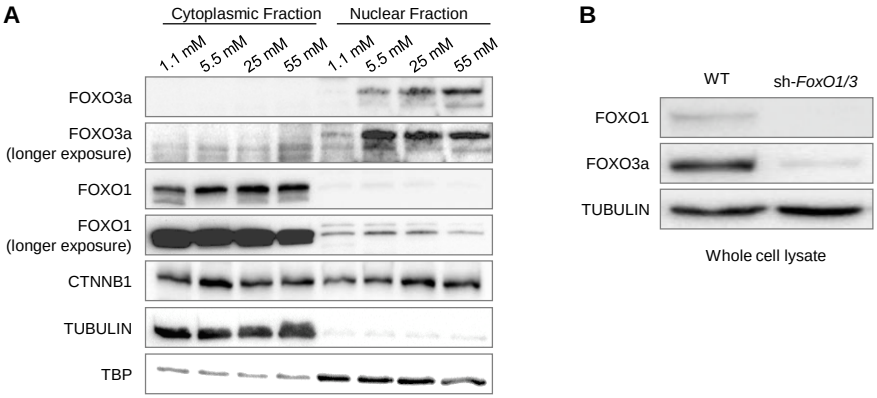

Supplemental Fig. 3

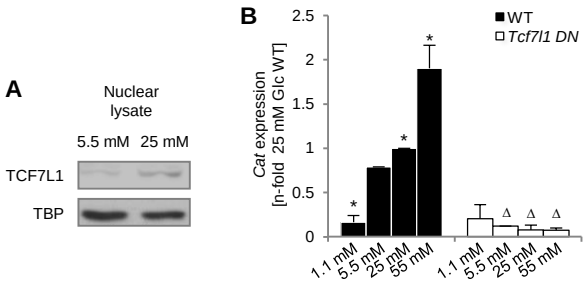

Supplemental Fig. 4